Available online at www.sciencedirect.com
ScienceDirect
Journal of Power Sources 170 (2007) 291–296
JOURNAL OF POWER SOURCES
www.elsevier.com/locate/jpowsour

Short communication

Ir_xCo_{1-x} ($x = 0.3$–1.0) alloy electrocatalysts, catalytic activities, and methanol tolerance in oxygen reduction reaction

Kunchan Lee, Lei Zhang, Jiujun Zhang *

Institute for Fuel Cell Innovation, National Research Council of Canada, 4250 Wesbrook Mall, Vancouver, BC, Canada V6T 1W5

Received 24 January 2007; received in revised form 16 April 2007; accepted 17 April 2007
Available online 25 April 2007

Abstract

Novel methanol-tolerant catalysts for oxygen reduction reaction (ORR), Ir_xCo_{1-x}/C ($x = 0.3$–1.0), were synthesized by a conventional impregnation method. These carbon-supported catalysts showed particle sizes of 2.7–5.0 nm. The catalyst activity and the catalyzed ORR kinetics were characterized by cyclic voltammetry and rotating disk electrode methods. Among these Ir_xCo_{1-x}/C catalysts, the alloy with a formula of Ir_xCo_{1-x}/C with x value in the range of 0.7–0.8 exhibited the highest mass and specific activities. Compared to a Pt/C catalyst, these alloy catalysts have much stronger methanol tolerance in terms of ORR onset potential (or open-circuit potential). Based on the rotating disk electrode measurements, it was confirmed that these Ir_xCo_{1-x}/C alloy catalysts could catalyze a complete four-electron transfer reaction of oxygen to water. These results strongly suggest that the novel Ir–Co metal alloy catalysts synthesized in this work could be promising for DMFC cathodes.

Keywords: Iridium; Ir–Co alloy; Electrocatalyst; Oxygen reduction reaction (ORR); Methanol tolerance; Direct methanol fuel cell (DMFC)

1. Introduction

High cost and low reliability (or durability) are two major barriers which hinder the commercialization of the fuel cell systems [1]. The platinum (Pt)-based electrocatalysts used in proton exchange membrane (PEM) fuel cells, including direct liquid fuel cells such as direct methanol fuel cells (DMFCs), are the major contributors to the fuel cells' high cost, due to the limited resources and the high price of Pt. Furthermore, the Pt-based catalysts used as the cathode catalysts in direct liquid fuel cells have no tolerance for fuel (methanol) oxidation [2]. Therefore, cost-effective and fuel-tolerant non-Pt catalysts are highly desired. In the effort to explore new catalysts, binary-, tri- and tetra-metal alloy catalysts, as some of the major types of fuel cell catalysts, have been synthesized and have shown promising catalyst activity towards cathodic oxygen reduction reaction [3].

Among different types of PEM fuel cells, the DMFC is considered to be the technology closest to the goal of fuel cell commercialization, due to the high energy density of its methanol fuel. Another advantage that the DMFC has over a hydrogen PEM fuel cell is that methanol is a liquid at ambient conditions, which makes fuel distribution and storage much easier. However, low performance and high cost are the two major drawbacks of DMFCs. Methanol (MeOH) crossover is a considerable cause of low performance. MeOH permeating through the membrane from the anode to the cathode can react directly with the cathode catalyst and O_2 to decrease the cathode potential and reduce fuel efficiency. Therefore, a cathode catalyst which is inert to MeOH is highly desirable. As discussed above, the Pt-based catalysts currently used as state-of-the-art cathode electrocatalysts have high cost and low oxygen reduction reaction (ORR) selectivity in the presence of MeOH.

Non-Pt catalysts such as palladium (Pd)-based catalysts have shown promising catalytic activities and methanol tolerance properties [2,4,5]. However, Pd shows much lower stability in high electrode potential and strong acidic media than does Pt [2,4,6]. Compared to Pt- and Pd-based catalysts, there has been relatively little research done on iridium (Ir) and Ir-based catalysts for oxygen reduction reaction. Among platinum group metals, Ir is one of the most stable in acidic media [6] and it is less expensive than Pt [7]. Although Ir has lower activity towards ORR than does Pt, it is interesting to note that its activity towards MeOH oxidation is also much lower than that of Pt [8,9]. Recently, our group found that Ir–Se chalcogenide showed

* Corresponding author. Tel.: +1 604 221 3087; fax: +1 604 221 3001.
E-mail address: jiujun.zhang@nrc.gc.ca (J. Zhang).

0378-7753/$ – see front matter © 2007 Elsevier B.V. All rights reserved.
doi:10.1016/j.jpowsour.2007.04.043

enhanced ORR activity and high MeOH tolerance [10]. This encouraging result has inspired us to explore Ir-based catalysts further.

As part of the continuing effort in new catalyst exploration, several novel iridium–cobalt alloy catalysts supported on the carbon particles, abbreviated as Ir_xCo_{1-x}/C with x value in the range of 0.3–1.0, were synthesized in this paper. The electrocatalytic activities and methanol tolerance of these new catalysts were measured in an acidic solution in the presence of methanol. The effect of the composition ratio of Co and Ir, $(1-x)/x$, was also investigated.

2. Experimental

2.1. Chemical synthesis

Ir_xCo_{1-x}/C catalysts were prepared via the precipitation method (conventional impregnation method). The x (=0.3–1.0) in Ir_xCo_{1-x}/C represents the chemical stoichiometry of Ir in the compound. A well-distributed suspension of carbon black (Vulcan XC-72R), the mixture of carbon black (300 mg) and deionized water (300 mL), was ultrasonicated over 2 h. Note that the carbon black was previously treated with a concentrated nitric acid for 5 h. The iridium chloride hydrate (Sigma–Aldrich) and cobalt(II) nitrate hexahydrate (Alfa Aesar) were added into this suspension for the metal loading of 20 wt.%, (note that depending on selected x value in the alloy, the added relative quantities of iridium chloride hydrate and cobalt(II) nitrate hexahydrate were different), and this mixture containing metal salts was ultrasonicated and stirred constantly at 80 °C. 1 M NaOH solution was added into this mixture to adjust the pH to 10–11. After that, 250 mL of 0.1 M sodium borohydride ($NaBH_4$) was added to completely reduce the metal ions and the mixture was stirred for 2 h. The resulted powders were filtered, washed with deionized water, and dried at 90 °C overnight. The catalyst powders obtained were heat-treated at 300 °C in a tube furnace under the mixture gas of N_2 and H_2 (9:1) for 2 h.

2.2. Instrumental characterization of the catalysts

The average chemical compositions for Ir_xCo_{1-x}/C alloy catalysts were determined by energy dispersive X-ray (EDX) analysis. The metal loadings of the catalysts obtained and of commercially available Ir supported on carbon particle, abbreviated as Ir/C (E-TEK), were determined by thermogravimetric analysis (TGA, TA Instruments). The sample powders were heated in a Pt pan up to 650 °C at a rate of 10 °C min^{-1} under air atmosphere.

For catalyst particle structure characterization, X-ray diffraction (XRD) measurements were carried out by Bruker D8 Advance X-ray diffractometer with Cu $K\alpha_1$ radiation. The XRD patterns were recorded between 20° and 90° at a step of 0.02°. The powder diffraction file database from the International Centre for Diffraction Data was used as a reference to interpret the peak assignments of the XRD spectra.

2.3. Electrode preparation and electrochemical measurements

The catalyst ink, a well-mixed suspension of Ir_xCo_{1-x}/C and deionized water, consisted of 1.0 mg mL^{-1} of catalyst. For the electrode coating process, a 12 μL of catalyst ink with 17 to 18 μg cm^{-2} of metal loading was pipetted onto the glassy carbon (GC) disk electrode (geometric area of 0.164 cm^2), and the coated electrode was left in the air to dry. For comparison, the catalyst inks for commercially available Ir/C (E-TEK) and Pt/C (E-TEK) were also separately prepared and coated on the electrodes.

A reversible hydrogen electrode (RHE) and Pt wire were used as the reference and the counter electrodes, respectively. Aqueous solutions of 0.5 M H_2SO_4 both with and without 0.5 M MeOH were used as the electrolytes. The electrochemically active surface areas of the Ir/C and Ir_xCo_{1-x}/C catalysts coated GC electrodes were evaluated by hydrogen adsorption/desorption charges on the recorded surface cyclic voltammograms and a well-reported charge value of hydrogen adsorption/desorption (220 μC cm^{-2}) [11]. Electrochemical measurements were conducted using a Pine instrument rotator and potentiostat equipped with a rotating glassy carbon disk-platinum ring electrode. All measurements were carried out at ambient conditions.

3. Results and discussion

3.1. Physical characterization

Table 1 shows the average chemical composition and metal loading for Ir_xCo_{1-x}/C and Ir/C catalysts. The metal loading in the catalyst powders was in the range of 23–25 wt.% for both Ir/C and Ir_xCo_{1-x}/C. However, the metal loading determined by

Table 1
Chemical compositions, metal loadings, and the structural parameters of Ir/C and Ir_xCo_{1-x}/C catalysts

Catalyst	Atomic ratio by EDX (Ir:Co)	Metal loading by TGA (wt.%)	Ir (2 2 0) peak position (°)	Lattice parameter a_{fcc} (Å)	Ir–Ir distance d (Å)	Particle size by XRD (nm)
Ir/C E-TEK	100	23.8	68.50	3.871	2.737	3.4
$Ir_{0.8}Co_{0.2}$/C	80.1:19.9	23.9	69.53	3.821	2.702	5.0
$Ir_{0.7}Co_{0.3}$/C	70.2:29.8	23.4	69.73	3.811	2.695	3.8
$Ir_{0.6}Co_{0.4}$/C	60.4:39.6	23.6	69.76	3.810	2.694	3.6
$Ir_{0.5}Co_{0.5}$/C	50.2:49.8	23.5	70.52	3.774	2.669	2.5
$Ir_{0.3}Co_{0.7}$/C	34.8:65.2	25.1	72.23	3.696	2.613	2.7

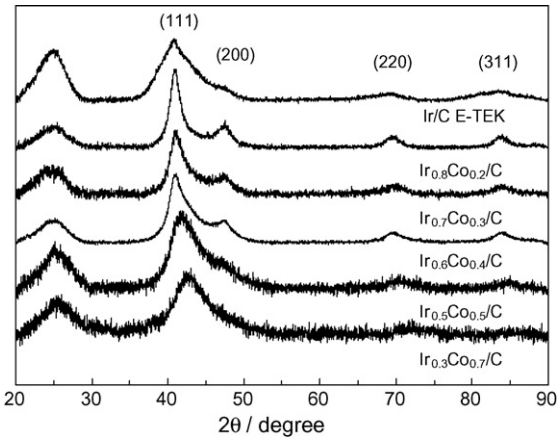

Fig. 1. X-ray diffraction patterns for Ir/C and Ir_xCo_{1-x}/C catalysts.

TGA is slightly higher than that expected from the feed loading, which was 20 wt.%. This result well agrees with the literature, indicating that some parts of metals might be oxidized in the TGA analysis [12]. Therefore, it could be expected that the actual metal loading is lower than the TGA-determined data.

In order to confirm that the synthesized catalysts are alloys, XRD patterns of Ir_xCo_{1-x}/C powders were collected and compared with that of Ir/C, as shown in Fig. 1. The first peaks located at ~25°, observed in all of the XRD patterns, can be assigned to the carbon support particles. The other peaks correspond to the face-centered cubic (fcc) crystalline of Ir, indicated by the planes of (1 1 1), (2 0 0), (2 2 0), and (3 1 1) at 41°, 47°, 69°, and 83°, respectively. This result may suggest that all of the Ir_xCo_{1-x} (x = 0.3–0.8) alloys have a single-phase disordered structure, i.e. a solid solution. This conclusion is supported by fact that there are no Co- and/or Co-oxide-associated peaks observed in the patterns of Fig. 1.

With respect to the morphology of the Ir_xCo_{1-x}/C alloys, Table 1 summarizes the structural parameters obtained by XRD analysis. The particle size was calculated by Scherrer's equation [13]. The peak position of the (2 2 0) plane of Ir increases with increasing Co content in Ir_x–Co_{1-x}/C alloys, resulting in the decrease of the lattice parameter and the Ir–Ir interatomic distance. This observation, together with the average chemical composition data in Table 1, may suggest that Ir could be alloyed with Co to form a solid solution.

3.2. Cyclic voltammetric characterization

Fig. 2(a) shows the representative cyclic voltammograms (CVs) for Ir/C and $Ir_{0.7}Co_{0.3}$/C catalysts in 0.5 M H_2SO_4 solutions with and without 0.5 M MeOH under N_2 atmosphere. The $Ir_{0.7}Co_{0.3}$/C catalyst displays surface electrochemical behaviour similar to that of Ir/C. The hydrogen adsorption/desorption ($H_{a/d}$) peaks can be observed in the potential range between 0.05 and 0.4 V versus RHE [6,14]. However, the $Ir_{0.7}Co_{0.3}$/C catalyst shows a decreased $H_{a/d}$ peak size compared to that of Ir/C, suggesting that the electrochemical active surface (EAS) may be decreased. The EASs for both Ir/C and Ir–Co alloy catalysts can be determined based on the chargers under the hydrogen adsorption/desorption peaks [11]. Table 2 shows the EASs obtained from cyclic voltammograms.

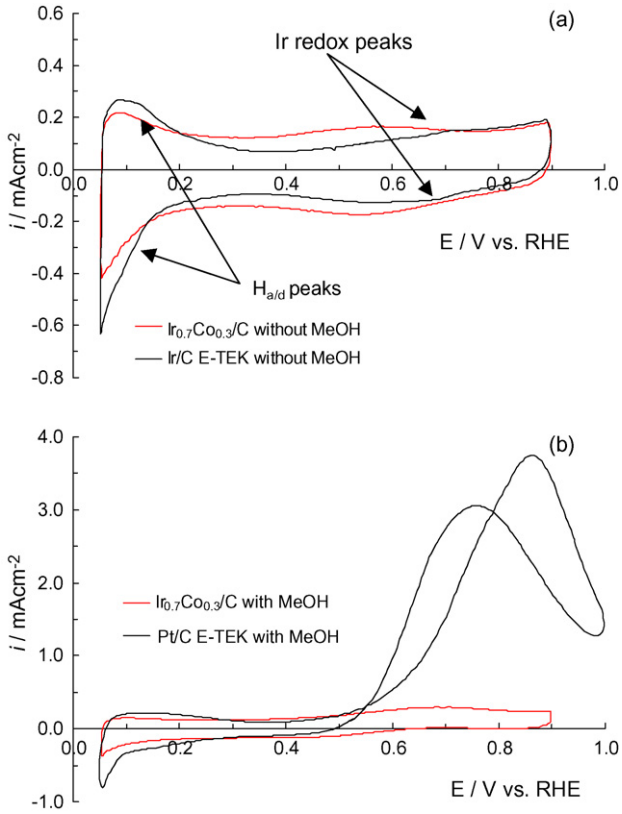

Fig. 2. Cyclic voltammograms for (a) $Ir_{0.7}Co_{0.3}$/C and Ir/C (E-TEK) catalysts in 0.5 M H_2SO_4 without MeOH, and (b) $Ir_{0.7}Co_{0.3}$/C and Pt/C (E-TEK) catalysts in 0.5 M H_2SO_4 with 0.5 M MeOH under saturated N_2. The current densities were normalized to the geometric area. Potential scan rate: 50 mV s^{-1}. 25 °C.

It has been reported that the adsorption characteristics of oxygen species such OH or O from water on an Ir electrode is much different from that of an oxygen species on a Pt electrode. The electrochemically oxidized Ir species exist in various oxidation states which are strongly dependent on electrode potential, electrolyte, and pre-treatment [14,15]. The oxygen species can be formed from 0.4 V versus RHE; their behaviour with respect to the formation and reduction process of Ir oxide is reversible below ~1.0 V versus RHE. When potential is greater than ~1.0, this process becomes irreversible. In our study, the electrode potential was employed between 0.05 and 0.9 V versus RHE in order to avoid the formation of irreversible Ir oxide. In this potential range, the Ir catalytic activities towards ORR and MeOH oxidation may be lower than those in the area beyond ~1.0 V [10,15]. For the Ir/C catalyst, a reversible peak corresponding to IrOH was observed at 0.7 V versus RHE on the CVs (Fig. 2(a)), which is consistent with the literature [14,15]. However, the $Ir_{0.7}Co_{0.3}$/C catalyst did not exhibit a clear redox peak at the same potential, indicating that the adsorption of oxygen species might be weakened.

For the methanol tolerance test, Fig. 2(b) shows the activity of the $Ir_{0.7}Co_{0.3}$/C catalyst towards MeOH oxidation. Compared to the Pt/C catalyst, the $Ir_{0.7}Co_{0.3}$/C catalyst displayed a negligible activity towards MeOH oxidation. This result indi-

Table 2
Tafel slopes and kinetic specific current densities

	Ir/C E-TEK	$Ir_{0.8}Co_{0.2}$/C	$Ir_{0.7}Co_{0.3}$/C	$Ir_{0.6}Co_{0.4}$/C	$Ir_{0.5}Co_{0.5}$/C	$Ir_{0.3}Co_{0.7}$/C
ESA ($m^2\ g_{Ir}^{-1}$)	18.2	5.1	10.1	7.7	9.2	9.4
Tafel slope (mV $dec.^{-1}$)	108	108	108	109	107	114
i_k at 0.7 V (mA cm^{-2})	0.135	0.425	0.322	0.396	0.298	0.319
i_k at 0.8 V (mA cm^{-2})	0.019	0.059	0.044	0.056	0.042	0.041

cates that Ir–Co alloy catalysts have a strong methanol tolerance property.

3.3. Electrocatalytic activity towards ORR

Fig. 3 shows the polarization curves of Ir_xCo_{1-x}/C catalysts towards ORR in an O_2-saturated 0.5 M H_2SO_4 solution. For comparison, the curve for the Ir/C (E-TEK) catalyst was also plotted under the same conditions. All the current densities were normalized to the geometric area and metal loading. Most of the Ir_xCo_{1-x} alloy catalysts showed enhanced ORR activities over that of the pure Ir catalyst, except for $Ir_{0.3}Co_{0.7}$/C. In terms of mass activity based on the metal loading, the $Ir_{0.7}Co_{0.3}$/C catalyst demonstrated the highest activity towards ORR among the alloys.

According to rotating disk electrode theory [16], the current density (i) at each electrode potential (E), shown in Fig. 3, should contain two contributions: the kinetic current density (i_k) and the diffusion current density (i_d). The relationship among these current densities can be expressed as Eq. (1):

$$i_k = i\left(\frac{i_d}{i_d - i}\right) \tag{1}$$

According to electrode kinetic theory [16], the kinetic current density can be expressed as a Tafel form,

$$\eta = a - \frac{2.3RT}{\alpha n F}\log(i_k) \tag{2}$$

where η is the overpotential, a is an exchange current density-related constant, R is the gas constant, T is the temperature, F is the Faraday constant, n is the electron transfer number in the determining step of the ORR, and α is the electron transfer coefficient. As shown in Fig. 4, according to Eq. (2) the Tafel plots for the kinetic current density normalized to the electrochemical active surface area between 0.7 and 0.9 V versus RHE. Ir_xCo_{1-x}/C alloy catalysts exhibited much better activities than did the pure Ir/C catalyst. As shown in Table 2, the Tafel slopes were ~110 mV $dec.^{-1}$ and the average αn obtained from these Tafel slopes was ~0.5, suggesting the electron transfer number in the determining step of the catalyzed ORR is 1 if α is assumed to be 0.5. Table 2 also shows that, in terms of specific activity, the $Ir_{0.8}Co_{0.2}$/C catalyst was the most active among the alloy catalysts.

In addition, the electrode rotating rate dependence of the catalyzed ORR current density was recorded to estimate the overall ORR electron number. According to the Koutecky–Levich theory [16], the diffusion current density in Eq. (1) can be expressed as Eq. (3):

$$i_d = 0.62nFCD^{2/3}\nu^{-1/6}\omega^{0.5} \tag{3}$$

where ω is the rotation rate of the disk electrode, n is the number of the transferred electrons in the overall reduction process, C is the concentration of O_2, D is the diffusion coefficient of the O_2, and ν is the kinematic viscosity. Fig. 5 shows the Koutecky–Levich plots for ORR on the $Ir_{0.7}Co_{0.3}$/C catalyst in 0.5 M H_2SO_4 with and without 0.5 M MeOH. The theoretical

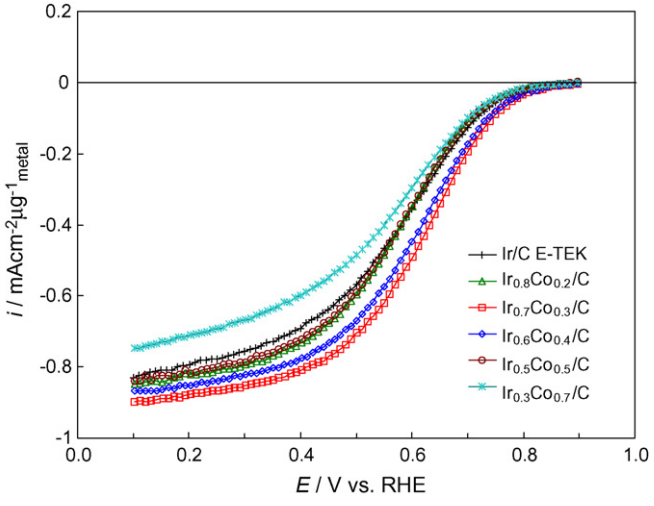

Fig. 3. Linear scan voltammograms for Ir/C and Ir_xCo_{1-x}/C catalysts in 0.5 M H_2SO_4 under saturated O_2. The current densities were normalized to the geometric area and metal loading. Potential scan rate: 5 mV s^{-1}. Electrode rotation rate: 400 rpm. 25 °C.

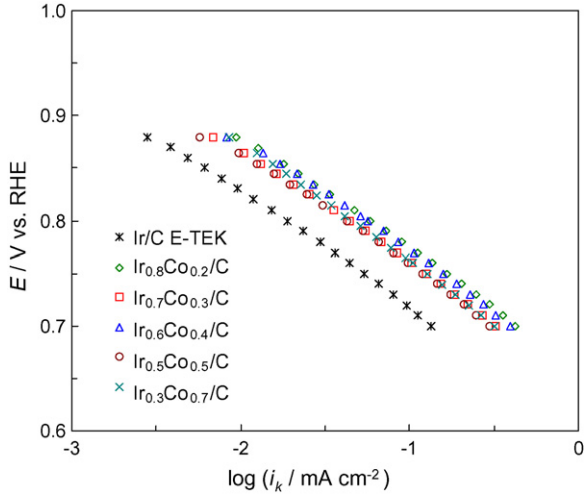

Fig. 4. Tafel plots for the ORR in 0.5 M H_2SO_4 under saturated O_2. The current densities were normalized to electrochemical active surface area. Potential scan rate: 5 mV s^{-1}. Electrode rotation rate: 400 rpm. 25 °C.

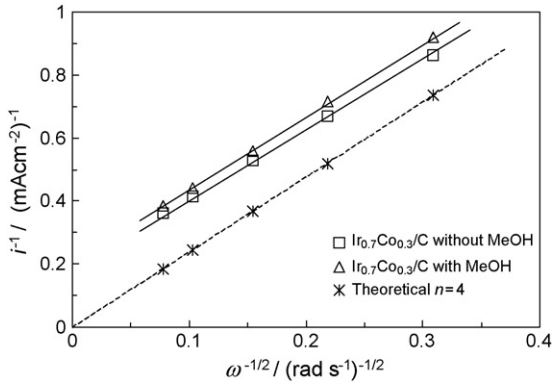

Fig. 5. Koutecky–Levich plots for the ORR on $Ir_{0.7}Co_{0.3}$/C catalyst at 0.5 V vs. RHE in saturated O_2 with and without 0.5 M MeOH. The current densities were normalized to the geometric area.

plot for a four-electron transfer process of ORR is also shown in Fig. 5. The parameters for the theoretical calculation were based on the experimental data reported by Ocampo et al. [17]. The plots both with and without MeOH give straight parallel lines, suggesting that the presence of methanol does not affect the ORR mechanism in terms of the electron transfer number. These two lines are parallel to the theoretically expected four-electron transfer plot, indicating that ORR catalyzed by the $Ir_{0.7}Co_{0.3}$/C catalyst is a four-electron transfer reaction from oxygen to water.

3.4. Methanol tolerance

In order to further test the methanol tolerance of the Ir_xCo_{1-x}/C catalysts, the catalyzed ORR was investigated in the presence of methanol, using the Pt/C catalyst for comparison. Fig. 6 compares the ORR polarization curves for Ir/C, $Ir_{0.7}Co_{0.3}$/C, and Pt/C with and without 0.5 M MeOH. The current densities were normalized to the geometric area and metal loading. In the absence of MeOH, the Pt/C catalyst shows significant ORR performance compared to the Ir/C and $Ir_{0.7}Co_{0.3}$/C catalysts. However, its performance dropped dramatically when MeOH was present, suggesting that the Pt/C catalyst has a very low ORR selectivity in the presence of MeOH. A large anodic current of Pt/C above 0.7 V versus RHE is due to the MeOH oxidation. The ORR onset potential for catalyzed ORR by Pt/C is around 0.7 V versus RHE, which is over 300 mV lower than that when MeOH is absent. Such an ORR onset potential drop can be attributed to the mixed potential caused by the simultaneous reaction of O_2 reduction and MeOH oxidation. For the $Ir_{0.7}Co_{0.3}$/C catalyst, the open-circuit potential (OCP) in the saturated O_2 atmosphere was ~0.9 V in the absence of MeOH, and no significant change in OCP was observed when MeOH was added to the electrolyte. The ORR performance was quite similar to that seen in the absence of MeOH, indicating that the Ir–Co/C catalyst has a high ORR selectivity in the presence of MeOH. In the presence of MeOH, the ORR onset potential of the $Ir_{0.7}Co_{0.3}$/C catalyst is ~130 mV higher that that of Pt/C, demonstrating that the $Ir_{0.7}Co_{0.3}$/C catalyst's ORR performance is superior to that of the Pt/C catalyst in terms of both ORR onset potential and current-potential performance (over 0.7 V versus RHE) in the presence of MeOH. These results suggest that Ir_xCo_{1-x}/C alloy catalysts have a strong methanol tolerance property and could be promising catalysts for DMFC cathodes.

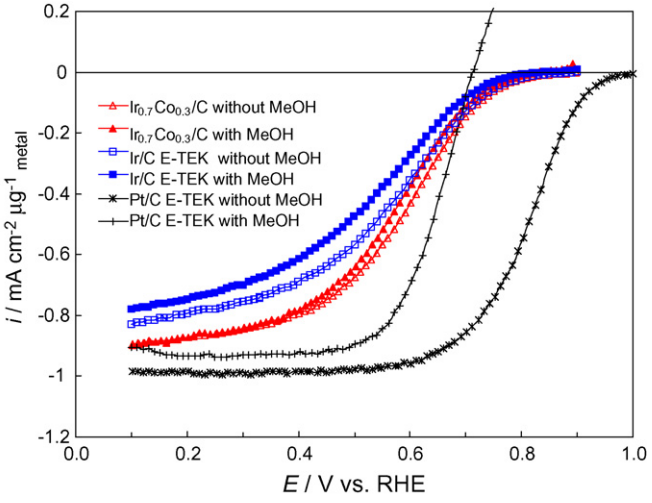

Fig. 6. Comparison of linear scan voltammograms for $Ir_{0.7}Co_{0.3}$/C, Ir/C (E-TEK), and Pt/C (E-TEK) in 0.5 M H_2SO_4 with and without 0.5 M MeOH under saturated O_2. The current densities were normalized to the geometric area and metal loading. Potential scan rate: 5 mV s^{-1}. Electrode rotation rate: 400 rpm. 25 °C.

4. Conclusions

Carbon-supported Ir–Co catalysts were synthesized. Instrumental analysis of the catalyst powders showed that these catalysts are fully alloying compounds between Ir and Co. The particle sizes of these alloying catalysts are around 2.7–5.0 nm, depending on the alloying degree.

Surface cyclic voltammetry and rotating disk electrode methods were used for the characterization of the catalyst activity and the catalyzed ORR kinetics. All the Ir_xCo_{1-x}/C alloy catalysts showed catalytic activities towards ORR in acidic solutions. In particular, the alloy with a formula of Ir_xCo_{1-x}/C with x value in the range of 0.7–0.8 exhibited the highest mass and specific activities. Compared to the Pt/C catalyst, these alloying catalysts have much stronger methanol tolerance in terms of ORR onset potential (or open-circuit potential) and performance over 0.7 V versus RHE. Based on the rotating disk electrode measurements, it was confirmed that these Ir_xCo_{1-x}/C alloy catalysts can catalyze a complete four-electron transfer reaction of oxygen to water. These results strongly suggest that the novel Ir-transition metal alloy catalysts synthesized in this work could be promising catalysts for DMFC cathodes. For Ir-based transition metal alloy catalysts, further study will involve the exploration of other second alloy elements.

Acknowledgements

This work is financially supported by the Institute for Fuel Cell Innovation, National Research Council of Canada (NRC-IFCI), and the Natural Sciences and Engineering Research Council of Canada (NSERC). The authors also want to

acknowledge the help of Dr. Ken Shi (NRC-IFCI) in physical characterization.

References

[1] DOE Fuel Cell Report to Congress (ESECS EE-1973), http://www1.eere.energy.gov/hydrogenandfuelcells/pdfs/fc_report_congress_feb2003.pdf.
[2] K. Lee, O. Savadogo, A. Ishihara, S. Mitsushima, N. Kamiya, K.-I. Ota, J. Electrochem. Soc. 153 (2006) A20.
[3] D. Thompsett, in: W. Vielstich, H.A. Gasteiger (Eds.), Handbook of Fuel Cells—Fundamentals, Technology and Applications, vol. 3, John Wiley & Sons, New York, 2003 (Chapter 37).
[4] J.L. Fernandez, D.A. Walsh, A.J. Bard, J. Am. Chem. Soc. 127 (2005) 357.
[5] M.-H. Shao, K. Sasaki, R.R. Adzic, J. Am. Chem. Soc. 128 (2006) 3526.
[6] D.A.J. Rand, R. Woods, J. Electroanal. Chem. 55 (1974) 375.
[7] Platinumtoday, http://www.platinum.matthey.com/publications/price_reports.html.
[8] A.J. Appleby, Catal. Rev. 4 (1970) 221.
[9] M.W. Breiter, Electrochim. Acta 8 (1963) 973.
[10] K. Lee, L. Zhang, J. Zhang, J. Power Sources 165 (2007) 108.
[11] B. Podlovchenko, G. Shterev, R. Semkova, E. Kolyadko, J. Electroanal. Chem. 224 (1987) 225.
[12] J. Luo, N. Kariuki, L. Han, L. Wang, C.-J. Zhong, T. He, Electrochim. Acta 51 (2006) 4821.
[13] V. Radmilovic, H.A. Gasteiger, P.N. Ross Jr., J. Catal. 154 (1995) 98.
[14] A. Aramata, T. Yamazaki, K. Kunimatsu, M. Enyo, J. Phys. Chem. 91 (1987) 2309.
[15] J. Mozota, B.E. Conway, Electrochim. Acta 28 (1983) 1.
[16] A.J. Bard, L.R. Faulkner, Electrochemical Methods: Fundamentals and Applications, 2nd ed., John Willey & Sons, New York, 2001 (Chapters 3 and 9).
[17] A.L. Ocampo, R.H. Castellanos, P.J. Sebastian, J. New Mater. Electrochem. Syst. 5 (2002) 163.